**Supporting Information:**

# Chemical Plausibility of Cu(III) with Biological Ligation in pMMO

Cooper Citek[1], J. Brannon Gary[1], Erik C. Wasinger[2] and T. Daniel P. Stack[1]*

*Corresponding Author

[1]Department of Chemistry, Stanford University, Stanford, CA 94305, USA

[2]Department of Chemistry, California State University, Chico, CA 95929, USA

**Table of Contents:**



**General Information:**

All chemicals were obtained from commercial sources if not mentioned otherwise. THF solvent was of HPLC grade and further purified by a Pure-Solv 400 solvent purification system (Innovative Technology) before storage over molecular sieves. 2-MeTHF (unstabilized, Aldrich) was dried with sodium/benzophenone and distilled under $N_2$ atmosphere before storage over molecular sieves. $[Cu(MeCN)_4]SbF_6$ was synthesized from $Cu_2O$ (Aldrich) and hexafluoroantimonic acid (Aldrich) by a variation of a literature method [1]. Preparation and manipulation of air-sensitive materials were carried out in a $N_2$ drybox (MBraun, <1 ppm in $O_2$ and $H_2O$). Low-temperature UV-Vis spectra were collected on a Varian Cary 50 Scan spectrophotometer with fiber-optic leads to a custom-designed quartz immersion probe (Hellma) of 0.1 cm optical path length in a custom-designed sample cell (ChemGlass). Reactions at -125°C were maintained by $N_2(l)$/pentane baths. $^1$H-NMR spectra were collected in $CDCl_3$ on either an Inova 300 MHz, Varian 400 MHz, or Mercury 400 MHz instrument. Reaction kinetics were followed by either single wavelength (363 nm) or multiwavelength (200 – 1000 nm) monitoring. Kinetic analyses were performed with SPECFIT 3.0.14 program. High resolution mass spectrometry measurements were performed by Stanford University Mass Spectrometry (SUMS) on a Bruker micrOTOF-Q II benchtop instrument. GC analyses were carried out on a HP5890A gas chromatograph with an Alltech EC-1 column (30 m x 0.53 x 1 μm) and FID detector.

**Preparation of Materials:**

All diamine ligands were obtained from Aldrich. Ligands were stirred over $CaH_2$ under $N_2$ atmosphere before vacuum distillation unless stated otherwise. Histamine free base was purchased from Matrix Scientific. 5,6-Isopropylidene-L-ascorbic acid (Aldrich) was dried in a vacuum oven before use. 10-Methyl-9-dihydroacridine and 10-methyl-9-dideutroacridine were prepared according to literature methods from 10-methylacridone[2] (TCI Chemicals); both were purified by sublimation before use. Dihydroanthracene (Aldrich) was recrystallized from ethanol before use. The tetradeuterated dihydroanthracene substrate was prepared according to literature methods [3]. 1,4 cyclohexadiene (Aldrich) was distilled from crushed molecular sieves before storage in the drybox. Xanthene (Aldrich) was purified by heated vacuum sublimation before

use. Dideuterated xanthene was prepared according to the same conditions, procedures, and purification as was tetradeuterated dihydroanthracene.

**Synthesis of $N_\alpha$,$N_\alpha$,$N_\tau$-trimethyl-histamine $L_3$:**

$N_\tau$-methyl-histamine dihydrochloride was synthesized from histamine free base through a cyclic urea intermediate [4]. $N_\alpha$-dimethylation was adopted from a known procedure [5]. In general, $N_\tau$-methyl-histamine dihydrochloride (1.0 g, 5 mmol), paraformaldehyde (1.5 g, 50 mmol), and sodium cyanoborohydride (3.1 g, 50 mmol) were stirred in 30 mL of 0.2 M $NH_4OAc_{(aq)}$ (pH 5.4) at 40°C overnight. Solid sodium hydroxide was added until the pH ≈ 13. The aqueous solution was extracted three times with 30 mL dichloromethane. The organic extracts were combined, dried over granular $Na_2SO_4$, and concentrated. The crude oil was stirred over crushed $CaH_2$ overnight before heated distillation under vacuum to give a clear viscous oil. Yield: 0.367 g, 52%. $^1$H-NMR(400 MHz, $CDCl_3$): δ 7.27 (s, 1H, aromatic H), δ 6.60 (s, 1H, aromatic H), δ 3.57 (s, 3H, $N_\tau$ methyl), δ 2.71-2.66 (mult., 2H, -$CH_2$-), δ 2.58-2.52 (mult., 2H, -$CH_2$-), δ 2.23 (s, 6H, $N_\alpha$ methyl). $^{13}$C-NMR(400 MHz, $CDCl_3$): δ 141.30, δ 137.19, δ 116.63, δ 59.63, δ 45.57, δ 33.57, δ 26.90. HRMS($H^+$): m/z = 154.1340 ($C_8H_{16}N_3$, calc. 154.1339).

**Synthesis of $N_\alpha$,$N_\alpha$-dimethyl-histamine $L_4$:**

Histamine (2.0 g, 18 mmol), paraformaldehyde (2.7 g, 90 mmol), and sodium cyanoborohydride (5.7 g, 90 mmol) were stirred in 60 mL of 0.2 M $NH_4OAc_{(aq)}$ (pH 5.4) at 40°C overnight. Solid sodium hydroxide was added until the pH ≈ 13. The aqueous solution was extracted four times with 30 mL dichloromethane. The organic extracts were combined, dried over granular $Na_2SO_4$, and concentrated. The crude oil was purified by heated distillation under vacuum to give a clear viscous oil. Yield: 0.763 g, 31%. $^1$H-NMR (400 MHz, $CDCl_3$): δ 7.47 (s, 1H, aromatic H), δ 6.75 (s, 1H, aromatic H), δ 2.78-2.69 (mult., 2H, $CH_2$), δ 2.59-2.52 (mult., 2H, $CH_2$), δ 2.27 (s, 6H, $N_\alpha$ methyl). $^{13}$C-NMR(400 MHz, $CDCl_3$): δ 134.52, δ 134.23, δ 119.23, δ 59.21, δ 45.31, δ 24.11. HRMS($H^+$): m/z = 140.1186 ($C_7H_{14}N_3$, calc. 140.1182).

**Synthesis of $N_\tau$-n-butyl-histamine $L_5$:**

$N_\tau$-n-butyl-histamine was synthesized from histamine free base according to the common method of $N_\tau$-alkylation through a cyclic urea intermediate[4]. 7,8-dihydro-6*H*-imidazo[1,5-*c*]pyrimidin-5-one (2.9 g, 21 mmol, CAS Registry Number: 14509-66-1) and iodobutane (4.3 g, 23 mmol) were stirred in 50 mL DMF at 40°C overnight. DMF solvent was removed under vacuum. The residue was refluxed in 40 mL of concentrated aqueous HCl overnight. A purple vapor indicating gaseous iodine was observed evolving from the refluxing mixture. The aqueous HCl was removed entirely by rotary evaporation, concurrent with sublimation of additional iodine. 20 mL of 4 M aqueous NaOH was added before extraction three times with 30 mL dichloromethane. The organic extracts were combined, dried over granular $Na_2SO_4$, and concentrated. The crude oil was stirred over crushed $CaH_2$ overnight before heated distillation under vacuum to give a clear viscous oil. Yield: 0.447 g, 13%. $^1$H-NMR(400 MHz, $CDCl_3$): δ 7.31 (s, 1H, aromatic H), δ 6.62 (s, 1H, aromatic H), δ 3.80 (t, 2H, -$CH_2$-), δ 2.92 (t, 2H, -$CH_2$-), δ 2.62 (t, 2H, -$CH_2$-), δ 1.67 (quint., 2H, -$CH_2$-), δ 1.25 (sext., 2H, -$CH_2$-), δ 0.87 (t, 3H, $CH_3$). $^{13}$C-NMR(400 MHz, $CDCl_3$): δ 140.74, δ 136.62, δ 115.79, δ 46.79, δ 42.06, δ 33.13, δ 32.57, δ 19.87, δ 13.64. HRMS($H^+$): m/z = 168.1499 ($C_9H_{18}N_3$, calc. 168.1495).

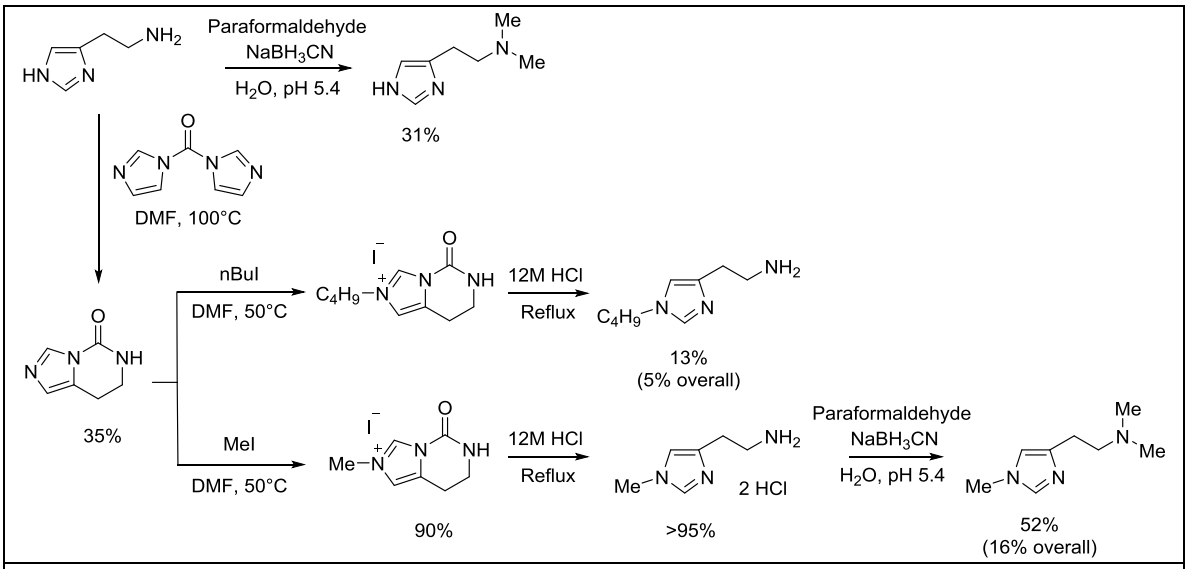


Scheme S1: Differential elaboration of histamine to yield **$L_3$-$L_5$**.

**General Method of Formation of 1-5:**

The optical immersion probe and reaction vessel described above were charged with 5 mL of purified and distilled 2-methyltetrahydrofuran (2MeTHF), sealed with a septum, and equilibrated in a $N_2(l)$/pentane frozen slurry (≈ -125°C). The vessel was purged with pure $O_2$ using a fine needle for *ca*. 10 min to saturate the solution. A 10 mM solution of $[Cu(CH_3CN)_4]SbF_6$ and TMPD in 500 µL of THF were injected slowly into the solution leading to formation of **1** after 10 min of stirring. The solution was sparged with $N_2$ gas using a fine needle for 10 min to remove excess dioxygen from the reaction vessel. Subsequently, 50 µL of 100 mM solution of $L_{2\text{-}5}$ (2 equiv) in 2MeTHF were added to effect the core capture of **1** to yield **2-5.**

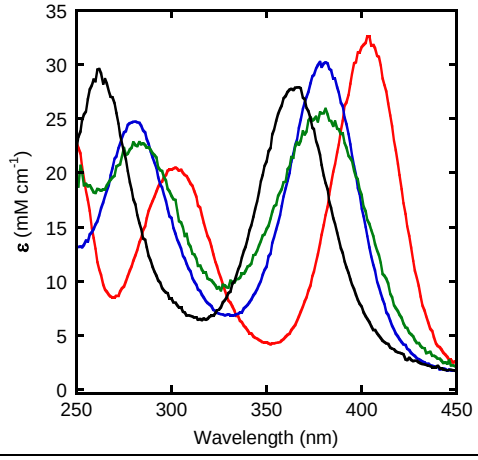


Figure S1**.** Absorption spectra of compounds **1** (red), **3** (blue), **4** (green), and **5** (black) in 2-MeTHF at -125°C ([Cu] ≈ 1 mM, 1 mm pathlength).

**Ligand competition experiments and stability rank:**

Complexes **1**, **2**, **3**, and **5** were formed by the method described above. To the equilibrated mixture, 50 µL of a 100 mM solution of the competing ligand (2 equiv of $\mathbf{L_2}$, $\mathbf{L_3}$, or $\mathbf{L_5}$) were added slowly. By observing changes in the optical spectrum and appearance and disappearance of characteristic absorption maxima, it was determined $\mathbf{L_5}$ can displace the ligands of **1** and **3**, $\mathbf{L_3}$ can displace the ligands of **1** and **2** but not **5**, $\mathbf{L_2}$ can displace the ligands of **1** but not **3**, and $\mathbf{L_1}$ is not capable of displacing the ligands of **2**, **3**, or **5**. In the situations in which the exogenous ligand could not effect core capture, excesses up to 6 equiv of ligand were added but typically lead to slow decay without detectable buildup of the exchanged complex. In some situations, exogenous ligands appear to be chemically incompatible with certain complexes, leading to decay (e.g. $\mathbf{L_5}$ in the presence of **2**). The successful experiments outlined provide sufficient data to establish the thermodynamic stability rank of complexes **1**, **2**, **3**, and **5** (i.e. **5** > **3** > **2** > **1**).

**Titrations of 3-5 with 5,6-Isopropylidene-L-ascorbic acid:**

**3-5** were formed by the method described above. Assuming a concentration [Cu] ≈ 0.9 mM, 1/10 equivalents of 5,6-isopropylidene-L-ascorbic acid ($2H^+/2e^-$ reductant) in THF were added. Each spectrum of the titrated species was allowed to stabilize (≈ 2 min) before addition of more titrant. The resulting titration spectra and absorbance versus equivalent plots are shown below. Titration data was used to established molar absorptivity and typical formation yield of complexes **3-5**. Lower bound estimates of formation yields from **1** are 75%, 60%, and 70% of complexes **3-5**, respectively.

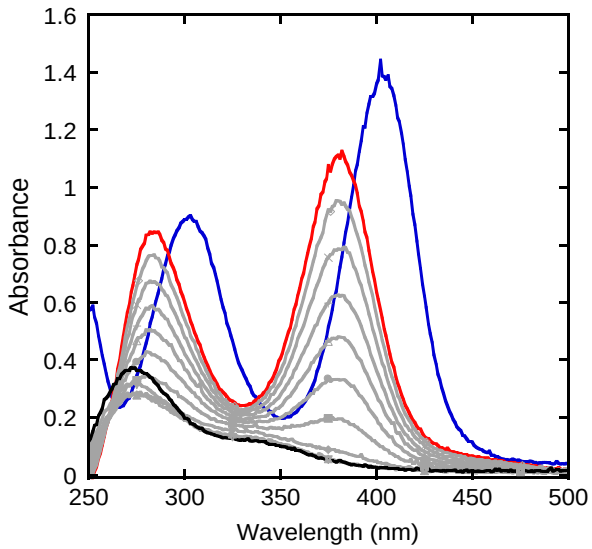


Figure S2. Spectra change of **3** (red) with incremental addition of 5,6-isopropylidene-L-ascorbic acid (grey) at -125°C, 2Me-THF. The blue spectrum corresponds to **1** used to form **3**.

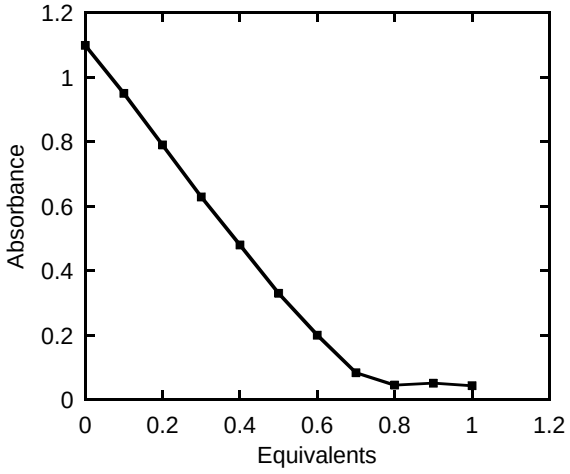


Figure S3. Titration plot of **3** with added 5,6-isopropylidene-L-ascorbic acid. Equivalents are relative to *ca.* 5 µmol Cu in 5.55 mL of solution.

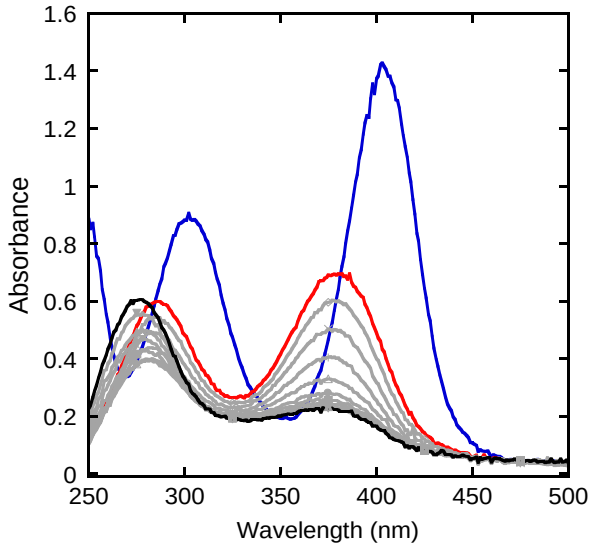


Figure S4. Spectra change of **4** (red) with incremental addition of 5,6-isopropylidene-L-ascorbic acid (grey) at -125°C, 2Me-THF. The blue spectrum corresponds to **1** used to form **4**.

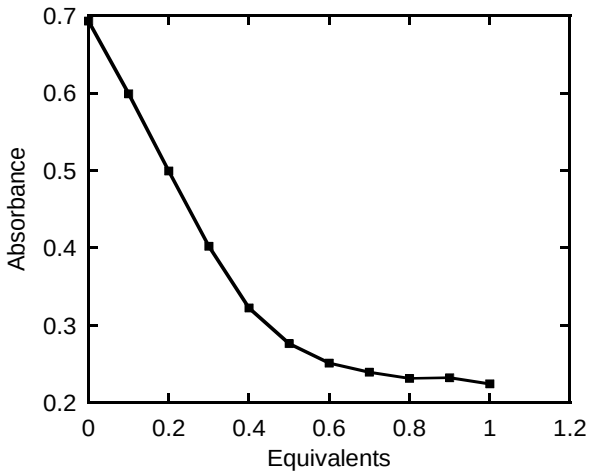


Figure S5. Titration plot of **4** with added 5,6-isopropylidene-L-ascorbic acid. Equivalents are relative to *ca.* 5 µmol Cu in 5.55 mL solution.

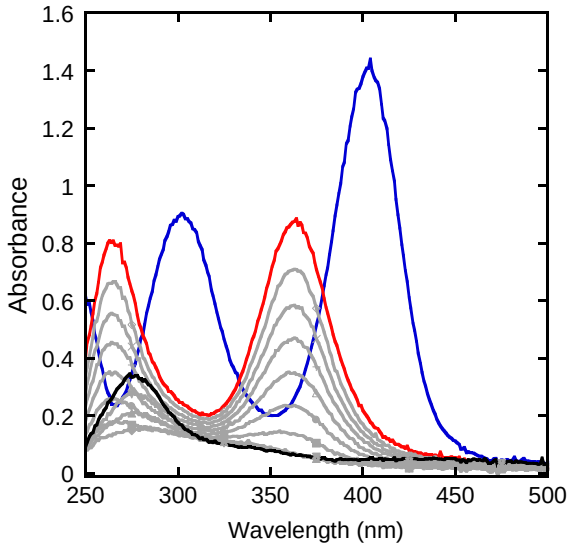


Figure S6. Spectra change of **5** (red) with incremental addition of titrant (grey) at -125°C, 2Me-THF. The blue spectrum corresponds to **1** used to form **5**.

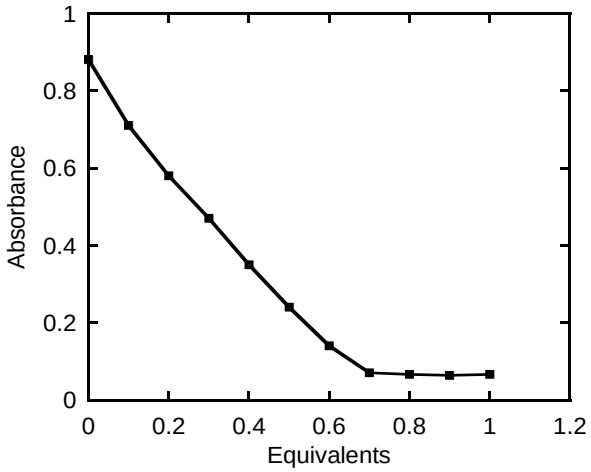


Figure S7. Titration plot of **5** with added 5,6-isopropylidene-L-ascorbic acid. Equivalents are relative to *ca.* 5 µmol Cu in 5.55 mL solution.

**Decay Kinetics of 5 with 10-methyl-9,10-dihydroacridine, $AcrH_2$:**

Compound **5** was formed by the method described above. 4-32 equivalents of 10-methyl-9,10-dihydroacridine in THF (maximum addition volume was 400 µL) were added quickly in one portion. The decay of **5** was recorded by single wavelength monitoring at its absorption maximum (363 nm). Absorption versus time decay data were fit by pseudo-first order kinetic

rates and plotted (Figure S8) against concentration of substrate to give the second order rate constant. The dehydrogenated product was identified by its characteristic UV absorptions[6].

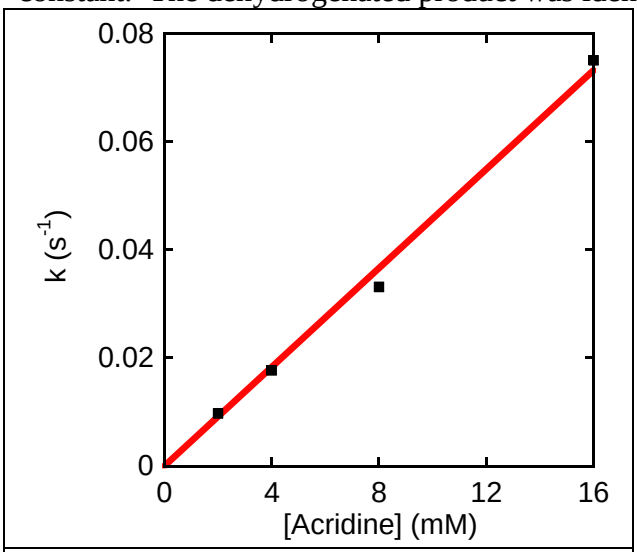


Figure S8. First-order dependence of the decay of **5** with 10-methyl-9,10-dihydroacridine at -125°C, 2Me-THF. $k = 4.6\ M^{-1}\ s^{-1}$. $R^2 = 0.9937$.

**Decay Kinetics of 5 with 1,4-cyclohexadiene:**

Compound **5** was formed by the method described above. 25-100 equivalents of 1,4-cyclohexadiene in THF were added quickly in one portion (maximum addition volume was 250 µL). The decay of **5** was recorded by monitoring the full absorption spectrum. Absorption versus time decay data were fit by pseudo-first order kinetic rates and plotted below against concentration of substrate to give the second order rate constant. Attempts to identify the products by GC were unsuccessful due to the large residual starting material and co-elution of solvent from the GC column.

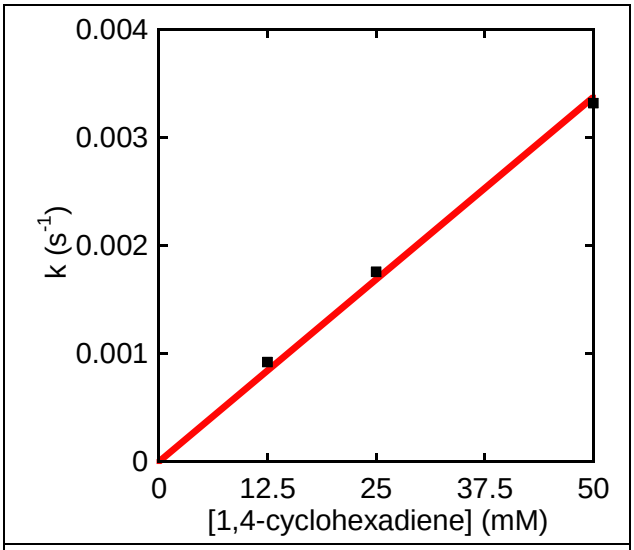


Figure S9. First-order dependence of the decay of **5** with 1,4-cyclohexadiene at -125°C,

2Me-THF. $k = 0.7 \times 10^{-1}\ M^{-1}\ s^{-1}$. $R^2 = 0.9950$.

**Decay Kinetics of 5 with Dihydroanthracene:**

Compound **5** was formed by the method described above. 25-100 equivalents of dihydroanthracene in THF were added quickly in one portion (maximum addition volume was 250 µL). The decay of **5** was recorded by monitoring the full absorption spectrum. Absorption versus time decay data were fit by pseudo-first order kinetic rates and plotted below against concentration of substrate to give the second order rate constant. Reactions were quenched at low temperature with 100 µL of 50% $NH_4OH_{(aq)}$ in MeOH. The mixture was passed through a Pasteur pipette column of basic alumina. The column was flushed with two volumes of MeOH. All volatile solvents were removed by rotary evaporation. The residue was taken up in THF, and the aromatized anthracene product was quantified by a calibrated GC method using the signal intensity ratio of anthracene to nitrobenzene internal standard. Anthracene product concentration was referenced to initial anthracene contamination concentration in the starting material, determined from control samples handled under identical conditions as product-containing reaction mixtures.

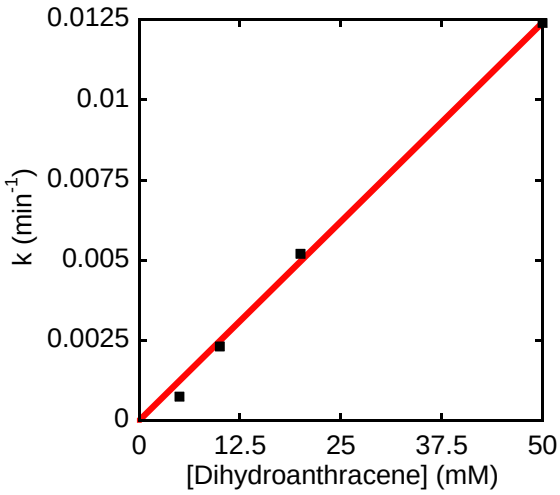


Figure S10. First-order dependence of the decay of **5** with dihydroanthrocene at -125°C, 2Me-THF. $k = 2.5 \times 10^{-1}\ M^{-1}\ s^{-1}$. $R^2 = 0.9960$.

**Decay Kinetics of 5 with Xanthene:**

Compound **5** was formed by the method described above. 25-100 equivalents of xanthene in THF were added quickly in one portion (maximum addition volume was 250 µL). The decay of **5** was recorded by monitoring the full absorption spectrum. Absorption versus time decay data were fit by pseudo-first order kinetic rates and plotted below against concentration of substrate to give the second order rate constant. Reactions were quenched at low temperature with 100 µL of 50% $NH_4OH_{(aq)}$ in MeOH. The mixture was passed through a Pasteur pipette column of basic alumina. The column was flushed with two volumes of MeOH. All volatile solvents were removed by rotary evaporation. The residue was taken up in THF, and the xanthone product was quantified by a calibrated GC method using the signal intensity ratio of xanthone to nitrobenzene internal standard. The O-atom insertion product xanthone was only

detected from reactions carried out in $O_2$ saturated solvent, in ca. 50% yields, consistent with dioxygen trapping of a xanthene radical intermediate before rearrangement to the product {Larsen, 2002 #11580}.

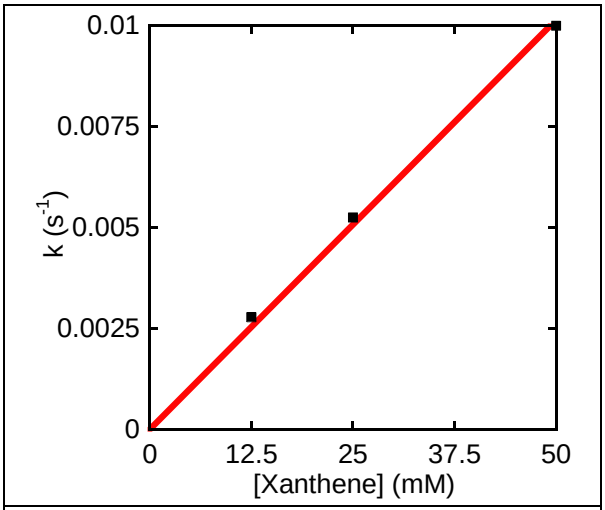


Figure S11. First-order dependence of the decay of **5** with xanthene at -125°C, 2Me-THF. $k = 2.0 \times 10^{-1}\ M^{-1}\ s^{-1}$. $R^2 = 0.9970$.

**Computational Details:**

*Full Bibliography of Gaussian 09:*

Gaussian 09, Revision D.01, Frisch, M. J.; Trucks, G. W.; Schlegel, H. B.; Scuseria, G. E.; Robb, M. A.; Cheeseman, J. R.; Scalmani, G.; Barone, V.; Mennucci, B.; Petersson, G. A.; Nakatsuji, H.; Caricato, M.; Li, X.; Hratchian, H. P.; Izmaylov, A. F.; Bloino, J.; Zheng, G.; Sonnenberg, J. L.; Hada, M.; Ehara, M.; Toyota, K.; Fukuda, R.; Hasegawa, J.; Ishida, M.; Nakajima, T.; Honda, Y.; Kitao, O.; Nakai, H.; Vreven, T.; Montgomery, J. A., Jr.; Peralta, J. E.; Ogliaro, F.; Bearpark, M.; Heyd, J. J.; Brothers, E.; Kudin, K. N.; Staroverov, V. N.; Kobayashi, R.; Normand, J.; Raghavachari, K.; Rendell, A.; Burant, J. C.; Iyengar, S. S.; Tomasi, J.; Cossi, M.; Rega, N.; Millam, J. M.; Klene, M.; Knox, J. E.; Cross, J. B.; Bakken, V.; Adamo, C.; Jaramillo, J.; Gomperts, R.; Stratmann, R. E.; Yazyev, O.; Austin, A. J.; Cammi, R.; Pomelli, C.; Ochterski, J. W.; Martin, R. L.; Morokuma, K.; Zakrzewski, V. G.; Voth, G. A.; Salvador, P.; Dannenberg, J. J.; Dapprich, S.; Daniels, A. D.; Farkas, Ö.; Foresman, J. B.; Ortiz, J. V.; Cioslowski, J.; Fox, D. J. Gaussian, Inc., Wallingford CT, 2009..

**TD-DFT Predicted Absorption Spectra of Compounds 1 and 3-5:**

Geometry optimizations and TD-DFT of the structures of **1** and **3-5** were performed in $C_i$ symmetry at a m06/TZVP level of theory using an SMD (THF) solvation model with Gaussian 09. The $C_i$ symmetry requires the ligands of **3-5** to be in an *anti* configuration with respect to each other. The electronic energies of optimized *syn* configurations are within 1 kcal $mol^{-1}$ of those of the *anti* configuration. The Natural Transition Orbitals[7] for the 2 major ligand-to-metal

charge transfer bands (LMCT) of **3-5** are presented below (Figure S12). The n-butyl substituent on $\mathbf{L}_5$ was truncated to a methyl group for calculations.

Table S1:
XYZ coordinates for optimized **1** in $C_i$ symmetry

| | | | |
|---|---|---|---|
| Cu | -0.06479800 | 1.41318300 | 0.00000000 |
| Cu | 0.06479800 | -1.41318300 | 0.00000000 |
| O | 0.00000000 | 0.00000000 | 1.12853100 |
| O | 0.00000000 | 0.00000000 | -1.12853100 |
| N | 0.00000000 | 2.68713300 | -1.54193600 |
| N | 0.00000000 | 2.68713300 | 1.54193600 |
| N | 0.00000000 | -2.68713300 | 1.54193600 |
| N | 0.00000000 | -2.68713300 | -1.54193600 |
| C | -0.48159500 | 4.05990100 | 1.25015700 |
| C | -0.82332600 | 2.15431900 | -2.64608500 |
| C | -0.82332600 | 2.15431900 | 2.64608500 |
| C | 0.82332600 | -2.15431900 | 2.64608500 |
| C | 0.48159500 | -4.05990100 | -1.25015700 |
| C | -1.41643100 | -2.70449400 | 1.96227100 |
| C | -0.48159500 | 4.05990100 | -1.25015700 |
| C | 1.41643100 | 2.70449400 | 1.96227100 |
| C | -1.41643100 | -2.70449400 | -1.96227100 |
| C | 0.48159500 | -4.05990100 | 1.25015700 |
| C | 0.82332600 | -2.15431900 | -2.64608500 |
| C | 1.41643100 | 2.70449400 | -1.96227100 |
| C | 0.07807700 | 4.68262900 | 0.00000000 |
| C | -0.07807700 | -4.68262900 | 0.00000000 |
| H | -1.57161900 | 4.00484200 | 1.17346500 |
| H | -0.24432700 | 4.67225000 | 2.12848800 |
| H | 0.77098500 | -2.84475800 | 3.49427900 |
| H | 0.45237500 | -1.17756400 | 2.94933900 |
| H | 0.24432700 | -4.67225000 | -2.12848800 |
| H | 0.24432700 | -4.67225000 | 2.12848800 |
| H | 0.77098500 | -2.84475800 | -3.49427900 |
| H | 1.85820700 | -2.06209200 | -2.31644000 |
| H | 0.45237500 | -1.17756400 | -2.94933900 |
| H | -0.24432700 | 4.67225000 | -2.12848800 |
| H | -1.57161900 | 4.00484200 | -1.17346500 |
| H | 1.73239000 | 1.68990000 | 2.20325500 |
| H | 2.04798500 | 3.09536400 | 1.16435900 |
| H | 1.52476000 | 3.33853000 | 2.84844500 |
| H | -2.04798500 | -3.09536400 | -1.16435900 |
| H | -1.52476000 | -3.33853000 | -2.84844500 |
| H | -1.73239000 | -1.68990000 | -2.20325500 |
| H | -1.73239000 | -1.68990000 | 2.20325500 |
| H | -2.04798500 | -3.09536400 | 1.16435900 |
| H | -1.52476000 | -3.33853000 | 2.84844500 |
| H | -1.85820700 | 2.06209200 | 2.31644000 |
| H | -0.77098500 | 2.84475800 | 3.49427900 |
| H | -0.45237500 | 1.17756400 | 2.94933900 |
| H | -0.45237500 | 1.17756400 | -2.94933900 |
| H | -0.77098500 | 2.84475800 | -3.49427900 |
| H | -1.85820700 | 2.06209200 | -2.31644000 |
| H | 1.52476000 | 3.33853000 | -2.84844500 |
| H | 1.73239000 | 1.68990000 | -2.20325500 |

Table S2:
XYZ coordinates for optimized **3** in $C_i$ symmetry

| | | | |
|---|---|---|---|
| Cu | -0.55085500 | 1.26963000 | 0.07713100 |
| Cu | 0.55085500 | -1.26963000 | -0.07713100 |
| O | -1.05835900 | -0.45699800 | 0.06362700 |
| O | 1.05835900 | 0.45699800 | -0.06362700 |
| N | -1.79231400 | -4.53047000 | -0.11808300 |
| N | 1.79231400 | 4.53047000 | 0.11808300 |
| N | -0.24886300 | -3.00572900 | -0.05749000 |
| N | 0.24886300 | 3.00572900 | 0.05749000 |
| N | -2.42906600 | 1.90240600 | 0.15296700 |
| N | 2.42906600 | -1.90240600 | -0.15296700 |
| C | 0.36166400 | -4.21617700 | 0.16575800 |
| C | -1.54271400 | -3.22690800 | -0.22316900 |
| C | -0.60115900 | -5.17543600 | 0.12426200 |
| H | -2.29017900 | -2.47030500 | -0.40513100 |
| H | -0.54986400 | -6.24534200 | 0.24514400 |
| C | -0.36166400 | 4.21617700 | -0.16575800 |
| C | 1.54271400 | 3.22690800 | 0.22316900 |
| C | 0.60115900 | 5.17543600 | -0.12426200 |
| H | 2.29017900 | 2.47030500 | 0.40513100 |
| H | 0.54986400 | 6.24534200 | -0.24514400 |
| C | 1.82467100 | -4.30764800 | 0.38057000 |
| H | 2.07599500 | -4.15545900 | 1.43537600 |
| H | 2.15964800 | -5.31789800 | 0.13743400 |
| C | -1.82467100 | 4.30764800 | -0.38057000 |
| H | -2.07599500 | 4.15545900 | -1.43537600 |
| H | -2.15964800 | 5.31789800 | -0.13743400 |
| C | 2.58845900 | -3.34195000 | -0.49687000 |
| H | 3.66168900 | -3.55869200 | -0.43826000 |
| H | 2.28102800 | -3.45586100 | -1.53924800 |
| C | -2.58845900 | 3.34195000 | 0.49687000 |
| H | -3.66168900 | 3.55869200 | 0.43826000 |
| H | -2.28102800 | 3.45586100 | 1.53924800 |
| C | -3.09198600 | -5.16558400 | -0.23684700 |
| H | -3.33663400 | -5.68219200 | 0.69092700 |
| H | -3.84101600 | -4.40074500 | -0.43188500 |
| H | -3.08207200 | -5.88089100 | -1.05867500 |
| C | 3.09198600 | 5.16558400 | 0.23684700 |
| H | 3.84101600 | 4.40074500 | 0.43188500 |
| H | 3.33663400 | 5.68219200 | -0.69092700 |
| H | 3.08207200 | 5.88089100 | 1.05867500 |
| C | -3.14648500 | 1.11442700 | 1.17410300 |
| H | -3.07589800 | 0.05524800 | 0.93510500 |
| H | -2.69831300 | 1.29584600 | 2.15154200 |
| H | -4.19745300 | 1.42012500 | 1.19051500 |
| C | 2.98461600 | -1.60849900 | 1.18255900 |
| H | 4.01988100 | -1.96127000 | 1.23384000 |
| H | 2.95366900 | -0.53309700 | 1.35094900 |
| H | 2.39552200 | -2.10290100 | 1.95509600 |
| C | 3.14648500 | -1.11442700 | -1.17410300 |
| H | 2.69831300 | -1.29584600 | -2.15154200 |

| | | | |
|---|---|---|---|
| H | 1.85820700 | -2.06209200 | 2.31644000 |
| H | 2.04798500 | 3.09536400 | -1.16435900 |
| H | -0.22273100 | 5.73293900 | 0.00000000 |
| H | 1.17135500 | 4.68904900 | 0.00000000 |
| H | 1.57161900 | -4.00484200 | -1.17346500 |
| H | 1.57161900 | -4.00484200 | 1.17346500 |
| H | -1.17135500 | -4.68904900 | 0.00000000 |
| H | 0.22273100 | -5.73293900 | 0.00000000 |

Table S3:

XYZ coordinates for optimized **4** in $C_i$ symmetry

| | | | |
|---|---|---|---|
| Cu | -0.34438300 | 1.34291100 | 0.04014000 |
| Cu | 0.34438300 | -1.34291100 | -0.04014000 |
| O | -1.12113900 | -0.27987500 | -0.03202800 |
| O | 1.12113900 | 0.27987500 | 0.03202800 |
| N | -2.47881700 | -4.17221400 | -0.29698400 |
| N | 2.47881700 | 4.17221400 | 0.29698400 |
| N | -0.72359100 | -2.92266500 | -0.13037400 |
| N | 0.72359100 | 2.92266500 | 0.13037400 |
| N | -2.10023200 | 2.27038200 | -0.02156300 |
| N | 2.10023200 | -2.27038200 | 0.02156300 |
| C | -0.33595000 | -4.21837600 | 0.12543000 |
| C | -2.02194400 | -2.92433800 | -0.37742400 |
| C | -1.43578400 | -5.00866100 | 0.01562100 |
| H | -2.61309100 | -2.05210000 | -0.60537100 |
| H | -1.56182300 | -6.07163500 | 0.13340000 |
| C | 0.33595000 | 4.21837600 | -0.12543000 |
| C | 2.02194400 | 2.92433800 | 0.37742400 |
| C | 1.43578400 | 5.00866100 | -0.01562100 |
| H | 2.61309100 | 2.05210000 | 0.60537100 |
| H | 1.56182300 | 6.07163500 | -0.13340000 |
| C | 1.07202900 | -4.54856300 | 0.44446100 |
| H | 1.26191300 | -4.44909900 | 1.51816900 |
| H | 1.25766400 | -5.59741200 | 0.20530600 |
| C | -1.07202900 | 4.54856300 | -0.44446100 |
| H | -1.26191300 | 4.44909900 | -1.51816900 |
| H | -1.25766400 | 5.59741200 | -0.20530600 |
| C | 2.04500300 | -3.71003600 | -0.35157700 |
| H | 3.06095600 | -4.10178100 | -0.22746400 |
| H | 1.79845700 | -3.75343300 | -1.41533300 |
| C | -2.04500300 | 3.71003600 | 0.35157700 |
| H | -3.06095600 | 4.10178100 | 0.22746400 |
| H | -1.79845700 | 3.75343300 | 1.41533300 |
| C | -3.01148200 | 1.59729200 | 0.92477100 |
| H | -3.07379300 | 0.53765500 | 0.68384000 |
| H | -2.62921100 | 1.71472800 | 1.93934500 |
| H | -4.00419800 | 2.05363500 | 0.85221800 |
| C | 2.59527200 | -2.09386200 | 1.40064900 |
| H | 3.54611200 | -2.62489900 | 1.51798100 |
| H | 2.74533700 | -1.03271500 | 1.59339900 |
| H | 1.87411600 | -2.48337100 | 2.11910700 |
| C | 3.01148200 | -1.59729200 | -0.92477100 |
| H | 2.62921100 | -1.71472800 | -1.93934500 |
| H | 3.07379300 | -0.53765500 | -0.68384000 |
| H | 4.00419800 | -2.05363500 | -0.85221800 |
| C | -2.59527200 | 2.09386200 | -1.40064900 |
| H | -2.74533700 | 1.03271500 | -1.59339900 |
| H | 3.07589800 | -0.05524800 | -0.93510500 |
| H | 4.19745300 | -1.42012500 | -1.19051500 |
| C | -2.98461600 | 1.60849900 | -1.18255900 |
| H | -2.95366900 | 0.53309700 | -1.35094900 |
| H | -4.01988100 | 1.96127000 | -1.23384000 |
| H | -2.39552200 | 2.10290100 | -1.95509600 |

Table S4:

XYZ coordinates for optimized **5** in $C_i$ symmetry

| | | | |
|---|---|---|---|
| Cu | -0.64180000 | 1.20616600 | 0.07871500 |
| Cu | 0.64180000 | -1.20616600 | -0.07871500 |
| O | -1.03215100 | -0.55065400 | 0.08668900 |
| O | 1.03215100 | 0.55065400 | -0.08668900 |
| N | -1.25240900 | -4.74316700 | -0.21935000 |
| N | 1.25240900 | 4.74316700 | 0.21935000 |
| N | 0.06012900 | -3.02019800 | -0.08906000 |
| N | -0.06012900 | 3.02019800 | 0.08906000 |
| N | -2.53530300 | 1.63667100 | 0.22800000 |
| N | 2.53530300 | -1.63667100 | -0.22800000 |
| H | 2.05191700 | 2.76003200 | 0.30549400 |
| C | 0.84975300 | -4.14408300 | -0.00341300 |
| C | -1.19689100 | -3.41230800 | -0.21608500 |
| C | 0.02964600 | -5.22475400 | -0.08684600 |
| H | -2.05191700 | -2.76003200 | -0.30549400 |
| H | 0.23901000 | -6.28210900 | -0.06177300 |
| C | -0.84975300 | 4.14408300 | 0.00341300 |
| C | 1.19689100 | 3.41230800 | 0.21608500 |
| C | -0.02964600 | 5.22475400 | 0.08684600 |
| H | -0.23901000 | 6.28210900 | 0.06177300 |
| C | 2.32129400 | -4.05805000 | 0.15900200 |
| H | 2.57741800 | -3.86535800 | 1.20868000 |
| H | 2.76880600 | -5.01969400 | -0.09615900 |
| C | -2.32129400 | 4.05805000 | -0.15900200 |
| H | -2.57741800 | 3.86535800 | -1.20868000 |
| H | -2.76880600 | 5.01969400 | 0.09615900 |
| C | 2.93363500 | -2.97531800 | -0.70212700 |
| H | 4.02373200 | -3.04446500 | -0.67183200 |
| H | 2.61629900 | -3.07035200 | -1.74218600 |
| C | -2.93363500 | 2.97531800 | 0.70212700 |
| H | -4.02373200 | 3.04446500 | 0.67183200 |
| H | -2.61629900 | 3.07035200 | 1.74218600 |
| H | -2.91296000 | 0.91051200 | 0.83460900 |
| H | -2.92124300 | 1.46694100 | -0.70164800 |
| H | 2.92124300 | -1.46694100 | 0.70164800 |
| H | 2.91296000 | -0.91051200 | -0.83460900 |
| C | -2.44780800 | -5.55620600 | -0.34548100 |
| H | -3.30397200 | -4.90331300 | -0.50061000 |
| H | -2.34775800 | -6.22849000 | -1.19672500 |
| H | -2.59702000 | -6.13886800 | 0.56316500 |
| C | 2.44780800 | 5.55620600 | 0.34548100 |
| H | 2.34775800 | 6.22849000 | 1.19672500 |
| H | 3.30397200 | 4.90331300 | 0.50061000 |
| H | 2.59702000 | 6.13886800 | -0.56316500 |

| | | | |
|---|---|---|---|
| H | -3.54611200 | 2.62489900 | -1.51798100 |
| H | -1.87411600 | 2.48337100 | -2.11910700 |
| H | 3.43758000 | 4.45455700 | 0.45030200 |
| H | -3.43758000 | -4.45455700 | -0.45030200 |

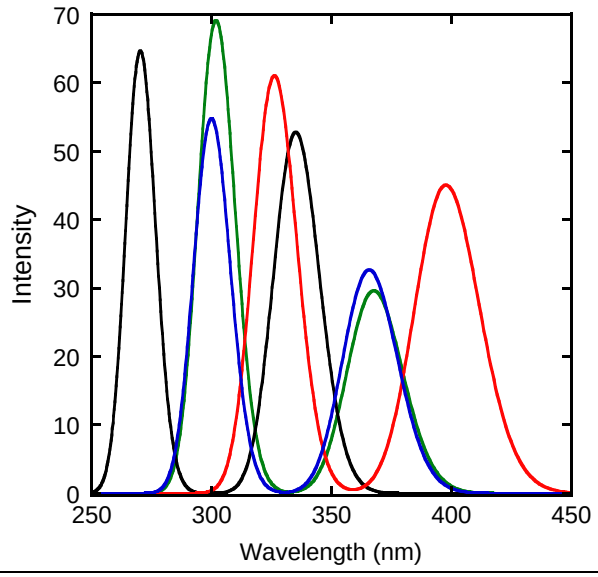


Figure S12. TD-DFT predicted spectra of compounds **1** (red), **3** (blue), **4** (green) and **5** (black), performed in $C_i$ symmetry at m06/TZVP/smd(THF) level of theory.

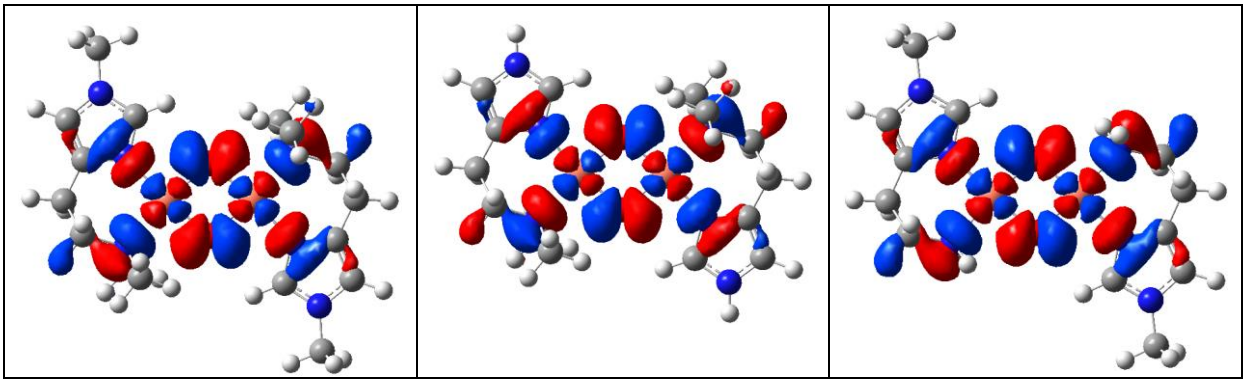

| | | |
|---|---|---|
| 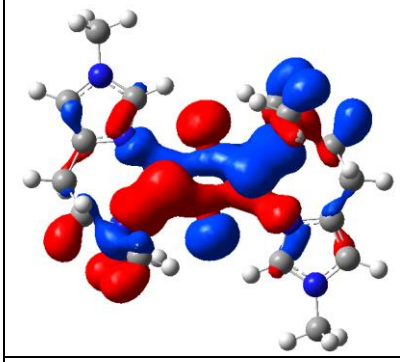 | 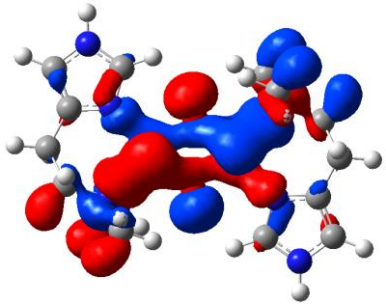 | 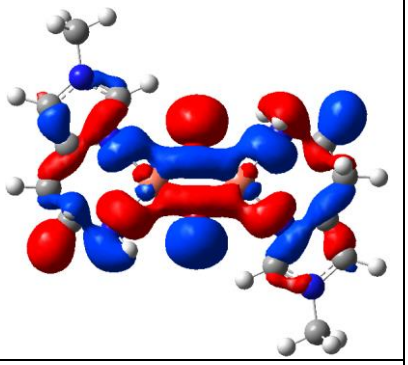 |
| Figure S13. NTO analysis of **3** Lower Energy LMCT (Top: acceptor, Bottom: Donor) | Figure S14. NTO analysis of **4** Lower Energy LMCT (Top: acceptor, Bottom: Donor) | Figure S15. NTO analysis of **5** Lower Energy LMCT (Top: acceptor, Bottom: Donor) |

| | | |
|---|---|---|
| 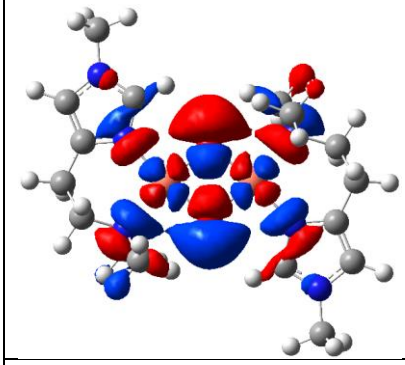 | 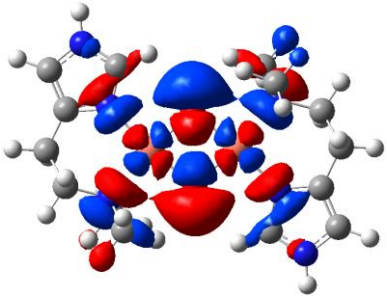 | 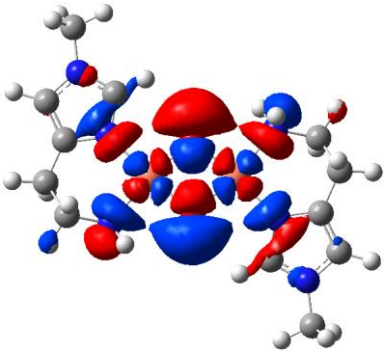 |
| 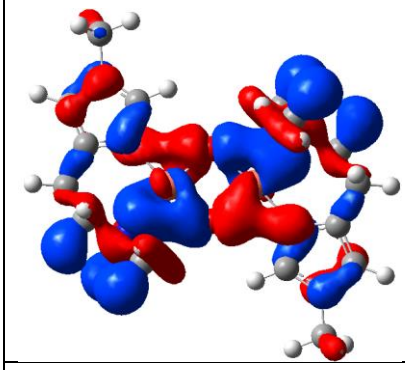 | 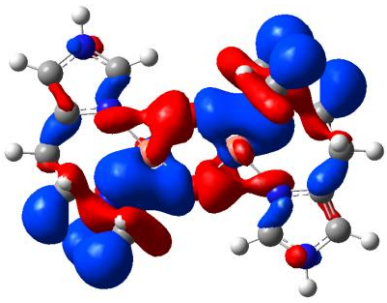 | 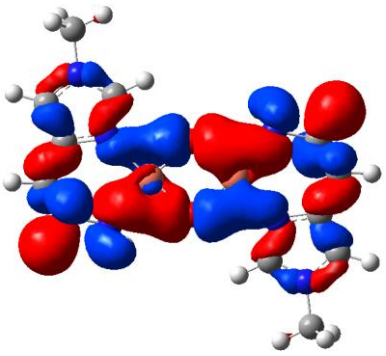 |
| Figure S16. NTO analysis of **3** Higher Energy LMCT (Top: acceptor, Bottom: Donor) | Figure S17. NTO analysis of **4** Higher Energy LMCT (Top: acceptor, Bottom: Donor) | Figure S18. NTO analysis of **5** Higher Energy LMCT (Top: acceptor, Bottom: Donor) |

**Transition State Analysis of 5 with 1,4-cyclohexadiene:**

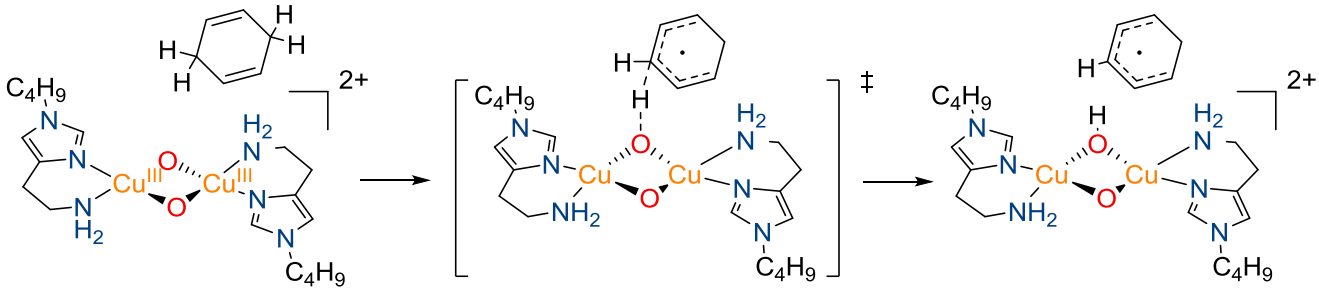


| $G_{173K}$ (kcal mol$^{-1}$) | | |
|---|---|---|
| restricted singlet | 7.6 | -12.5 |
| triplet | 23.6 | -27.0 |
| broken-symmetry singlet | 6.6 | -28.0 |

Figure S19. Calculated reaction profile for the C-H bond activation of 1,4-cyclohexadien by **5** (energy in kcal mol$^{-1}$).

The activation of the allylic C-H bond of 1,4-cyclohexadiene by the $Cu(III)_2O_2$ species (**5**) was simulated by density functional theory (DFT) using the Gaussian09 software package. Optimizations, single point calculations, and frequency calculations were performed in vacuum at an m06/SVP level of theory. Frequency calculations provided zero-point energies and thermodynamic corrections at 153 K for single point energy calculations (m06/SVP), which included SMD solvation (THF) and 2$^{nd}$ order relativistic corrections (DKH2). The n-butyl substituent on $\mathbf{L}_5$ was truncated to a methyl group to for the calculations. Only the structure of **5** in which the ligands were arranged in an *anti* configuration with respect to each other was considered.

The Gibbs energy at 153K of the structure **SM** was calculated as the sum of the individual restricted singlet energies of **5** and 1,4-cyclohexadiene and is used as a reference for the energy profile (Figure S19). The triplet state of **5** and 1,4-cyclohexadiene are significantly higher in energy and were not considered in this analysis. The **Int** structure was accessible from forward IRC (internal reaction coordinate) calculations from the transition states **TS**. The restrict singlet, broken-symmetry singlet, and triplet states of **Int** have a low-lying imaginary frequency. Minimum structure **SM** was confirmed by all positive frequencies, while the restricted singlet transition state **TS** has one and only one large, imaginary frequency. This imaginary frequency clearly exhibits a vibrational mode corresponding to the C-H bond cleavage along with a nearly linear alignment of the activated C-H bond and the H-accepting oxygen atom, similar to those observed in simulated C-H bond activation of methane by iron-oxide species[8].

In theory, the triplet state or anti-ferromagnetically coupled broken-symmetry singlet state of **TS** and **Int** may also be involved significantly in the reaction. All unrestricted triplet-state and broken-symmetry singlet geometry optimizations, however, failed to locate any stable transition state structures. As such, the triplet-state and broken-symmetry singlet energies were estimated by single-point calculations on the structures of the restricted singlet. The broken-symmetry transition state has one and only one imaginary frequency, while the triplet transition

state contains a second, low-lying frequency in addition to the major bond-breaking frequency. The spin-corrected approach reported by Yamaguchi *et al.*[9] was adapted to calculate the broken-symmetry energies.

At 153 K (-125°C), the activation of the allylic C-H bond is calculated to have a small barrier for a restricted or broken-symmetry singlet reaction (6.6 to 7.6 kcal $mol^{-1}$) and the overall process is thermodynamically downhill. A triplet transition state is calculated to be energetically inaccessible; the conservation of the spin ground state from **SM** to **TS** then to **Int** suggests that spin crossover is not significant and the reaction takes place via a singlet pathway. However the triplet state of **Int** is very close in energy to the broken-symmetry state. The calculated reaction profile clearly indicates that the barrier for $Cu^{III}_2O_2$ species (**5**) to cleave the allylic C-H bonds of 1,4-cyclohexadiene at -125°C is reasonable, consistent with the experimentally observed reactivity in solution.

The reaction profile in Figure S19 supports an H atom abstraction description of the reaction, in which an anti-ferromagnetically coupled singlet forms and is preferred over singlet hydride transfer. Inspection of the spin population of the broken-symmetry singlet **TS** show delocalization of spin on the Cu(II)-O-Cu(III) core fragment and on the forming cyclohexadiene radical (Figure S20). The most stable form of **Int** is a diamagnetically coupled complex with a cyclohexadienyl radical and a delocalized (O)(OH)-bridged Cu(II)Cu(III) core. The two moieties of **Int** communicate with each other presumably through an interaction between the O-H σ antibonding orbital and a cyclohexadienyl π bonding orbital as observed in its β SOMO (Figure S21).

In summary, the DFT calculations suggest that the first C-H bond activation of 1,4-cyclohexadiene by the $Cu^{III}_2O_2$ species (**5**) is overall a H-atom abstraction process, proceeding along a singlet manifold.

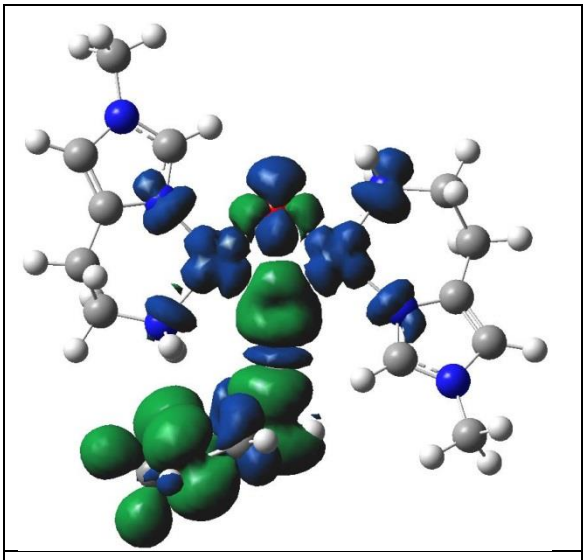

Figure S20. Calculated spin density of **TS** on broken-symmetry surface of cyclohexadiene reacting with **5**.

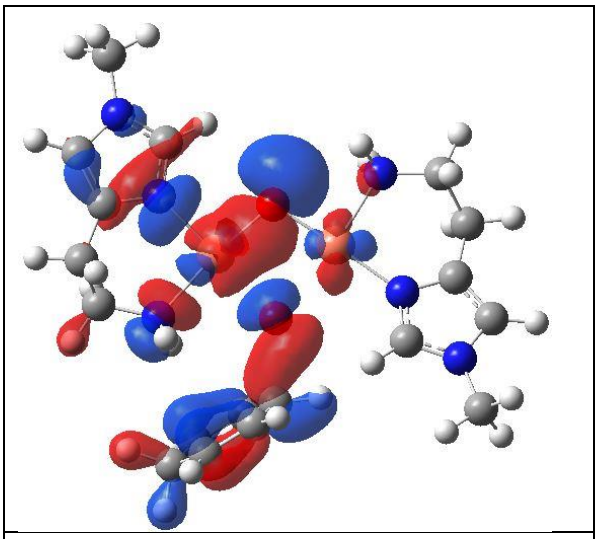

Figure S21: β SOMO of **Int** on broken-symmetry surface.

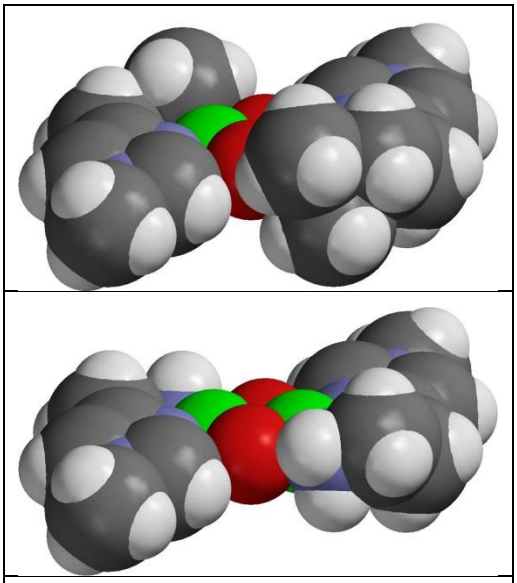

Figure 22: Space-filling models of 3 (Top) and 5 (Bottom). The n-butyl substituent of L5 is truncated to a methyl group.

**Thermodynamic Evaluation of Ligand Affinity:**

Thermodynamic evaluation of all structures was performed in the following manner: structures (complexes or ligands) were optimized in vacuum with m06/TZVP level of theory. Vacuum frequencies provided zero-point corrections and Gibbs energies on single point electronic calculations, which included SMD solvation (THF) and 2$^{nd}$ order relativistic corrections (DKH2). Appropriate arithmetic expressions were written to evaluate the calculated free energy change of ligand exchange reactions. A Hess' law relation holds for the energetics

of various combinations of complexes and exchanging ligands. The rank ordered stability of complexes **1**, **2**, **3**, and **5** is reproduced by calculations as detailed in Figure S23.

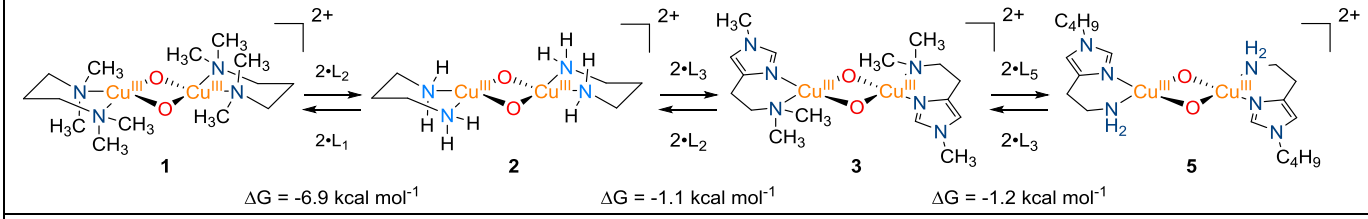


Figure S23: DFT computed ligand competition reaction energetics.

**Thermodynamic Evaluation of Standard Reduction Potential:**

Thermodynamic evaluation of all structures was performed in the following manner: structures were optimized in vacuum at an m06/TZVP level of theory. Vacuum frequencies provided zero-point corrections and Gibbs energies from single point electronic calculations, which included SMD solvation (Water) and 2nd order relativistic corrections (DKH2). The DFT method to evaluate relative standard reduction potentials was calibrated from $E_0$ of Cu(III)/Cu(II) reduction potentials of mononuclear polypeptide-chelated copper complexes from the classic work of Margerum (Figure S24) [10]. Relative $E_0$ values were calculated from the free energy change of balanced isodesmic reactions involving the single electron transfer between Cu(II) and Cu(III) species. These experimentally-calibrated copper-specific isodesmic reactions allow for favorable cancellation of systematic errors in the computation of Cu(II) and Cu(III) states.

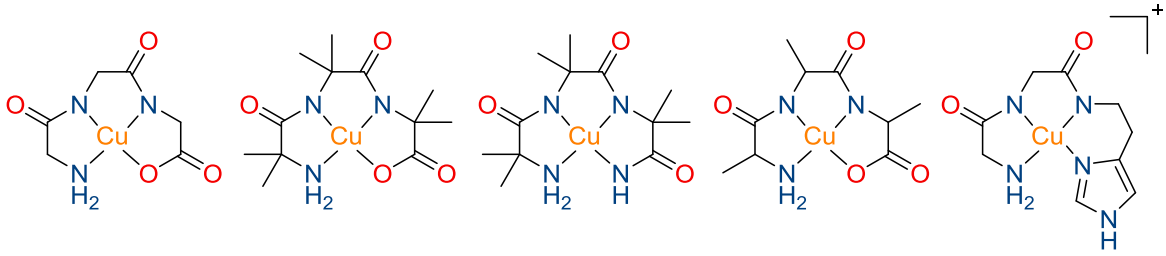


Figure S24: Mononuclear, polypeptide Cu(III) complexes. $E_0$ versus NHE measured in water at 298 K.

The calculated standard reduction potential of each mononuclear complex was first evaluated by an isodesmic electron transfer reaction between its Cu(III) state and Cu(II)Aib$_3$Amide, the reference complex. For each complex, the calculated standard reduction potential was taken as the sum of the experimental reduction potential of Cu(III)Aib$_3$Amide (0.37 V) and the calculated reaction free energy. Figure S25 shows a correlation between the experimentally determined and calculated standard reduction potentials.

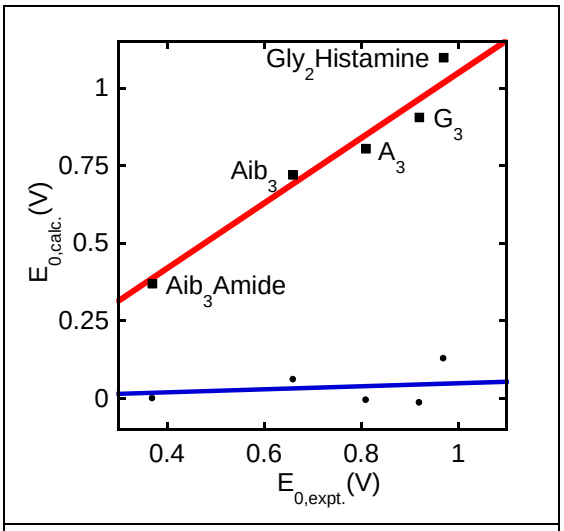


Figure S25: Calculated $E_0$ reduction potentials versus experimental $E_0$ of five of mononuclear Cu(III) peptide complexes of Margerum (Figure S24). $R^2 = 0.9544$ (red). Deviations of calculated from experimental values (blue).

Optimizations and energy evaluations of **5** ($C_i$ symmetry) and its $1e^-$ reduced form ($C_1$ symmetry) followed the method detailed above. The n-butyl substituent on $\mathbf{L_5}$ was truncated to a methyl group for calculations. Isodesmic electron transfer reactions were constructed between **5** and the Cu(II) state of each mononuclear complex. Reaction free energies were plotted against the experimental $E_0$ of each mononuclear complex. The calculated standard reduction potential of **5** was taken as the "x-intercept" of the linear fit in Figure S26 (750 mV vs NHE).

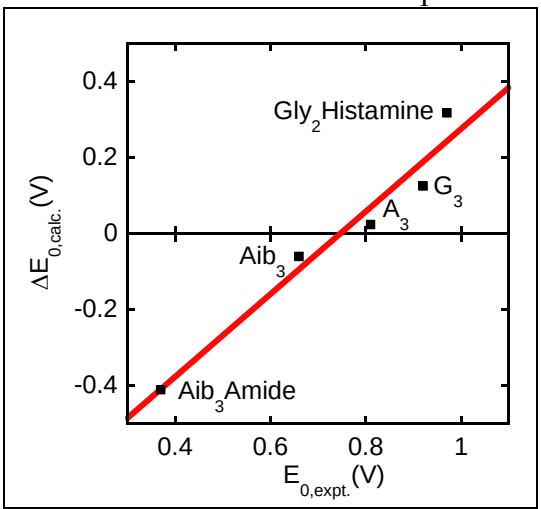


Figure S26: Isodesmic electron transfer reaction free energy versus experimental reduction potential. Fit $R^2 = 0.9558$.

**X-ray Absorption Spectroscopy (XAS):**

The samples were loaded into Lucite XAS cells with 37 μm Kapton windows by direct immersion of the cell into the solution at -125°C, frozen in liquid nitrogen ($LN_2$), and stored under $LN_2$ until use. Cu K-edge X-ray absorption data were collected on wiggler beam line 7-3 at the Stanford Synchrotron Radiation Lightsource under ring conditions of 3.0 GeV and 450-500 mA. A Si (220) monochrometer was used for energy selection and detuned 50% to minimize harmonic components of the X-ray beam. During data collection, samples were maintained at 10–15 K using an Oxford Instruments CF1208 continuous flow liquid helium cryostat. Data were measured in fluorescence mode, monitoring the Cu Kα fluorescence signal with a 30-element Ge solid-state array detector. Internal energy calibration was performed by simultaneous measurement of the transmission signal through a Cu reference foil. The first inflection point of the copper reference data was aligned to 8980.3 eV. Data represent averages of 8 scans of each sample. Photoreduction was monitored and only scans with main edge shifts of less than 0.5 eV were included in the final data averages. Data reduction was performed according to established methods[11].

The intensities and energies of the 1s→3d pre-edge features were quantified using pseudo-Voigt line-shapes to model the rising edge background and absorption features of the Cu complexes according to established methods[11]. For each complex, a series of 3 to 6 fits over varying energy ranges and with varying background features were performed and averaged using the program EDG_FIT[12]. The reported area values (FWHM*Amplitude*100) are the average for each of the fits to a given complex.

Theoretical EXAFS signals were calculated using structural models based on appropriate model complexes as input parameters to FeFF (version 7) [13] and fitted to the data using SIXPACK[14]. The structural parameters R (Å), the bond distance, and the bond variance, $\sigma^2$ ($Å^2$), were varied for all shells in all fits. The $\Delta E_0$ (eV) value representing the ionization threshold value was also varied for each fit, but was restrained to be a common value for all contributions within a given fit. EXAFS data were fit to k = 14 $Å^{-1}$ for all samples **3-5** in accordance with the noise level of the data. The structural parameters that were varied during the refinements include the bond distance (R) and the bond variance ($\sigma^2$). The $\sigma^2$ is related to the Debye-Waller factor, which is a measure of thermal vibration and static disorder of the absorbers and scatterers. Coordination numbers were systematically varied during the course of the analysis, but were not allowed to vary within a given fit.

It should be noted that the Cu-N-C multiple scattering waves (~3.20 Å, Table S1) for compounds **3** and **4** were found to have an exceptionally low Debye-Waller factor if the coordination number was fixed at 10 in the fits, as would be expected from the model. However, it was found that artificially expanding the coordination number up to 14 did not impact the overall fit. In such cases, the fit error changed immaterially (<0.005); none of the distances varied by more than 0.02 Å (the resolution of the experiment); the Debye-Waller values for the other waves varied by less than 10%; and the visual quality of the fit was unchanged. Alternatively, completely removing the wave increased the fit error by 50-100%. Therefore, the Cu-N-C multiple scattering wave is a necessary component of the fit, but the fit is invariant to differences in the contribution's coordination number to a large extent. Most importantly, in no case did this effect vary the Cu-O or Cu-N distances by more than 0.01 Å.

**Additional Acknowledgement**

Use of the Stanford Synchrotron Radiation Lightsource, SLAC National Accelerator Laboratory, is supported by the U.S. Department of Energy, Office of Science, Office of Basic Energy Sciences under Contract No. DE-AC02-76SF00515. The SSRL Structural Molecular Biology Program is supported by the DOE Office of Biological and Environmental Research, and by the National Institutes of Health, National Institute of General Medical Sciences (including P41GM103393). The contents of this publication are solely the responsibility of the authors and do not necessarily represent the official views of NIGMS or NIH.

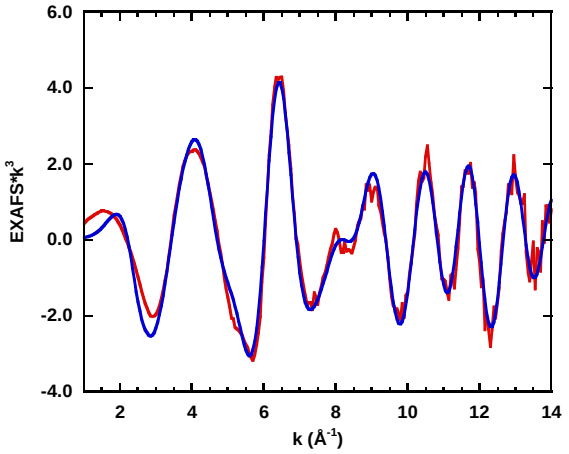


Figure S27: EXAFS (red) and Fit (blue) of **3**.

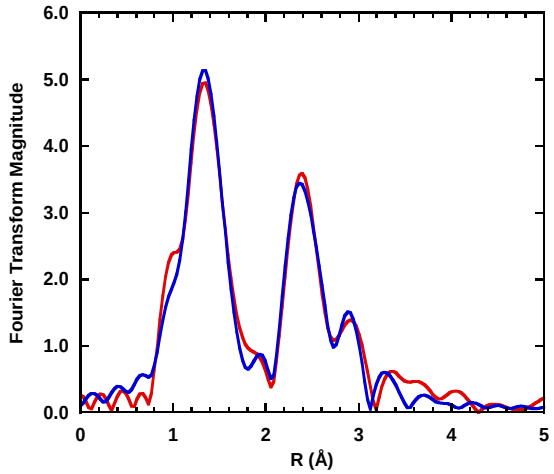


Figure S28: Fourier Transform of EXAFS (red) and Fit (blue) of **3**.

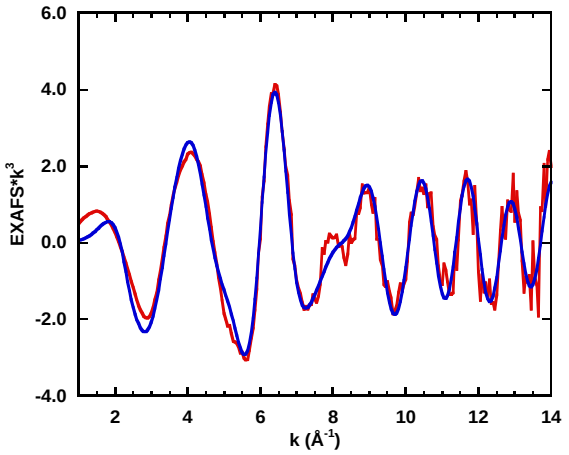


Figure S29: EXAFS (red) and Fit (blue) of **4**.

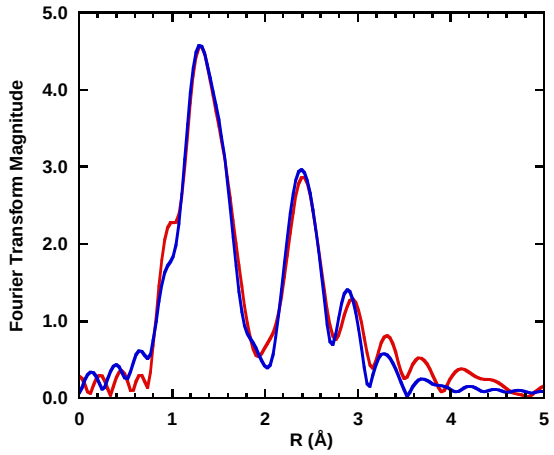


Figure S30: Fourier Transform of EXAFS (red) and Fit (blue) of **4**.

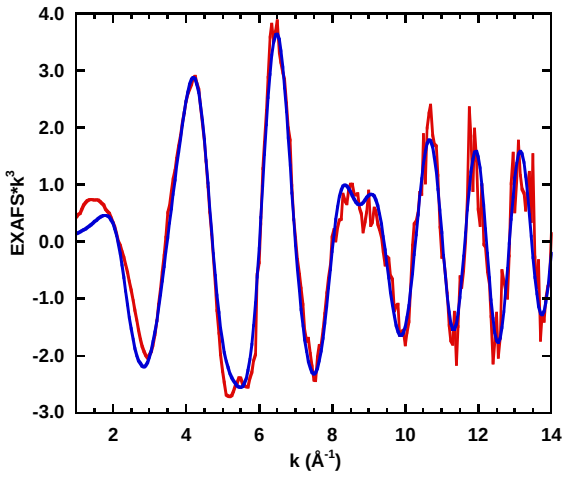


Figure S31: EXAFS (red) and Fit (blue) of **5**.

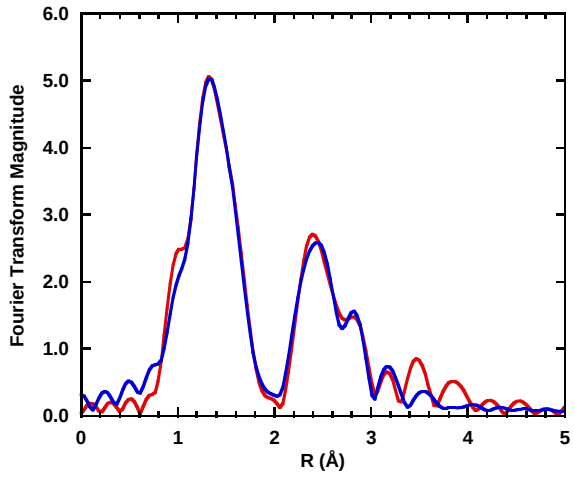


Figure S32: Fourier Transform of EXAFS (red) and Fit (blue) of **5**.

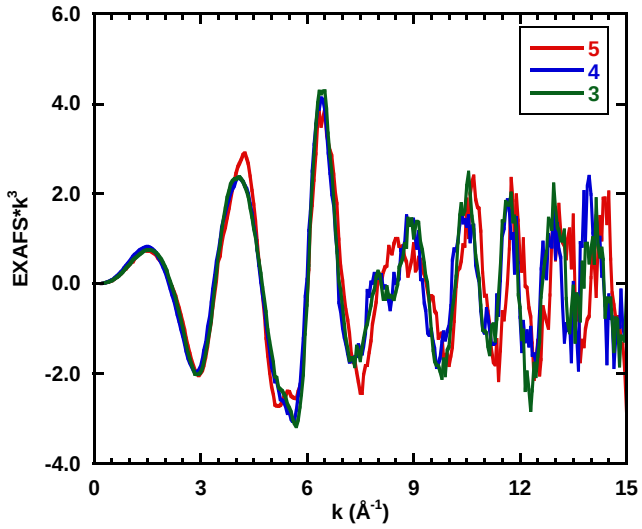


Figure S33: EXAFS overlay of **3**-**5**.

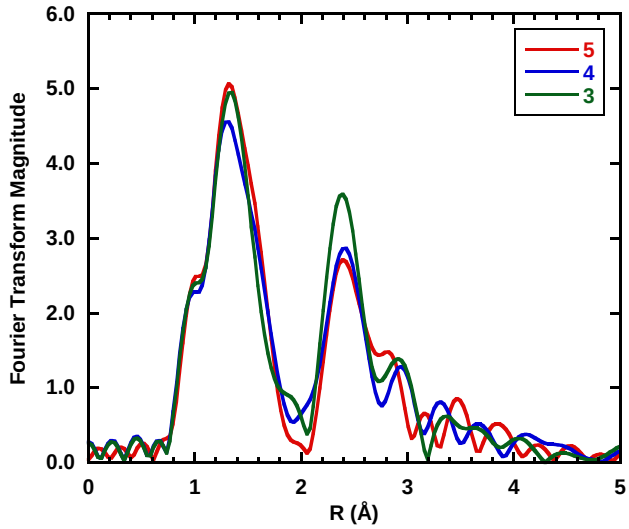


Figure S34: EXAFS fourier transform overlay of **3**-**5**.

| | **Complex 3** | $E_0$ | R (error) | **Complex 4** | $E_0$ | R (error) | **Complex 5** | $E_0$ | R (error) |
|---|---|---|---|---|---|---|---|---|---|
| k=1-14(1/Å) | | -10.5 | 0.0353 | | -12.2 | 0.0644 | | -10.5 | 0.0622 |
| | CN | R (Å) | DW (Å$^2$) | CN | R (Å) | DW (Å$^2$) | CN | R (Å) | DW (Å$^2$) |
| Cu-O | 2 | 1.82 | 0.00348 | 2 | 1.81 | 0.00461 | 2 | 1.82 | 0.00434 |
| Cu-N | 2 | 1.97 | 0.00308 | 2 | 1.96 | 0.00282 | 2 | 1.96 | 0.00321 |
| Cu-Cu | 1 | 2.80 | 0.00315 | 1 | 2.81 | 0.00365 | 1 | 2.78 | 0.00439 |
| Cu-C (SS) | 5 | 3.02 | 0.00602 | 5 | 3.03 | 0.00534 | 3 | 2.99 | 0.00079 |
| Cu-C (MS) | 14 | 3.21 | 0.00198 | 14 | 3.19 | 0.00195 | 6 | 3.16 | 0.00554 |
| Cu-N-C (MS) | 8 | 4.08 | 0.01523 | 8 | 4.07 | 0.01607 | 8 | 4.05 | 0.01726 |

Table S5: EXAFS determined metrical parameters of compounds **3-5**.

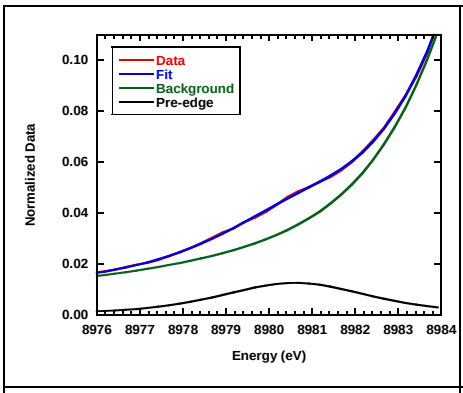


Figure S35: Fits to pre-edge data for **3** indicating a Cu(III) center absorbing at 8980.7 ± 0.4 eV.

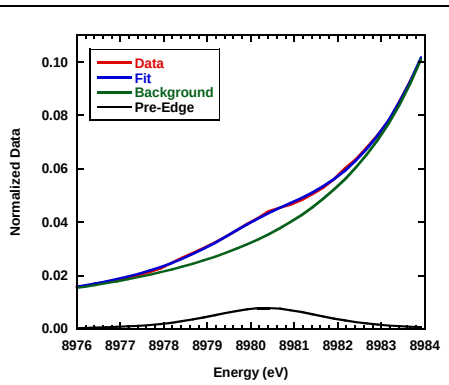


Figure S36: Fits to pre-edge data for **4** indicating a Cu(III) center absorbing at 8980.5 ± 0.1 eV.

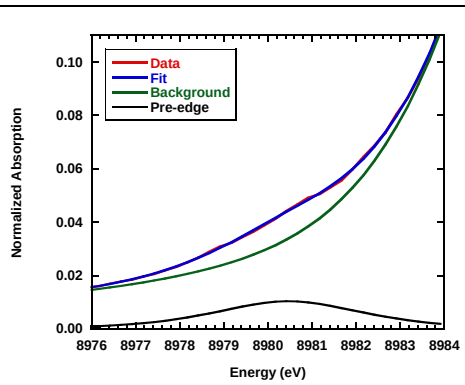


Figure S37: Fits to pre-edge data for **5** indicating a Cu(III) center absorbing at 8980.6 ± 0.2 eV.

**References:**


(1) Kubas, G. J.; Monzyk, B.; Crumbliss, A. L. *Inorg. Synth.* **1979**, *19*, 90.
(2) Manring, L. E.; Peters, K. S. *J. Am. Chem. Soc.* **1983**, *105*, 5708.
(3) Goldsmith, C. R.; Jonas, R. T.; Stack, T. D. P. *J. Am. Chem. Soc.* **2002**, *124*, 83.
(4) Saulnier, M. G.; Frennesson, D. B.; Wittman, M. D.; Zimmermann, K.; Velaparthi, U.; Langley, D. R.; Struzynski, C.; Sang, X.; Carboni, J.; Li, A.; Greer, A.; Yang, Z.; Balimane, P.; Gottardis, M.; Attar, R.; Vyas, D. *Bioorg. Med. Chem. Lett.* **2008**, *18*, 1702.
(5) Taki, M.; Teramae, S.; Nagatomo, S.; Tachi, Y.; Kitagawa, T.; Itoh, S.; Fukuzumi, S. *J. Am. Chem. Soc.* **2002**, *124*, 6367.
(6) Taki, M.; Itoh, S.; Fukuzumi, S. *J. Am. Chem. Soc.* **2001**, *123*, 6203.
(7) Martin, R. L. *J. Chem. Phys.* **2003**, *118*, 4775.
(8) Yoshizawa, K. *Coord. Chem. Rev.* **2002**, *226*, 251.
(9) Yamaguchi, K.; Jensen, F.; Dorigo, A.; Houk, K. N. *Chem. Phys. Lett.* **1988**, *149*, 537.
(10) *Redox Decomposition Reactions of Copper(III) Peptide Complexes*; Margerum, D. W.; Scheper, W. M.; McDonald, M. R.; Fredericks, F. C.; Wang, L.; Lee, H. D., Eds.; Chapman & Hall: New York, 1993.
(11) DuBois, J. L.; Mukherjee, P.; Stack, T. D. P.; Hedman, B.; Solomon, E. I.; Hodgson, K. O. *J. Am. Chem. Soc.* **2000**, *122*, 5775.
(12) George, G. N. Stanford, CA, 2000.
(13) Ankudinov, A. L.; Rehr, J. J. *Phys. Rev. B* **1997**, *56*, R1712.
(14) Webb, S. M. *Phys. Scr.* **2005**, *2005*, 1011.